

PolypGen: A multi-center polyp detection and segmentation dataset for generalisability assessment

Sharib Ali^{1,2,*}, Debesh Jha^{4,5}, Noha Ghatwary⁶, Stefano Realdon^{7, †}, Renato Cannizzaro^{9, †}, Osama E. Salem¹¹, Dominique Lamarque¹⁰, Christian Daul¹², Kim V. Anonsen¹⁶, Michael A. Riegler^{4,5}, Pål Halvorsen^{4,15}, Jens Rittscher¹, Thomas de Lange^{8,13,14 †}, and James E. East^{2,3, †}

¹Department of Engineering Science, Big Data Institute, University of Oxford, Oxford, UK

²NIHR Oxford Biomedical Research Centre, Oxford, UK

³Translational Gastroenterology Unit, Experimental Medicine Div., John Radcliffe Hospital, University of Oxford, Oxford, UK

⁴SimulaMet, Oslo, Norway

⁵Department of Computer Science, UiT The Arctic University of Norway

⁶Computer Engineering Department, Arab Academy for Science and Technology, Alexandria, Egypt

⁷Veneto Institute of Oncology IOV-IRCCS, Padua, Italy

⁸Medical Department, Sahlgrenska University Hospital-Möln达尔, Sweden

⁹CRO Centro Riferimento Oncologico IRCCS Aviano Italy

¹⁰Université de Versailles St-Quentin en Yvelines, Hôpital Ambroise Paré, France

¹¹Faculty of Medicine, University of Alexandria, Egypt

¹²CRAN UMR 7039, Université de Lorraine and CNRS, Vandœuvre-Lès-Nancy, France

¹³Department of Molecular and Clinical Medicine, Sahlgrenska Academy, University of Gothenburg, Sweden

¹⁴Augere Medical, Oslo, Norway

¹⁵Oslo Metropolitan University, Oslo, Norway

¹⁶Oslo University Hospital Ullevål, Oslo, Norway

*corresponding author: Sharib Ali (sharib.ali@eng.ox.ac.uk)

†these authors contributed equally to this work

ABSTRACT

Polyps in the colon are widely known as cancer precursors identified by colonoscopy either related to diagnostic work-up for symptoms, colorectal cancer screening or systematic surveillance of certain diseases. Whilst most polyps are benign, the number, size and the surface structure of the polyp are tightly linked to the risk of colon cancer. There exist a high missed detection rate and incomplete removal of colon polyps due to the variable nature, difficulties to delineate the abnormality, high recurrence rates and the anatomical topography of the colon. In the past, several methods have been built to automate polyp detection and segmentation. However, the key issue of most methods is that they have not been tested rigorously on a large multi-center purpose-built dataset. Thus, these methods may not generalise to different population dataset as they overfit to a specific population and endoscopic surveillance. To this extent, we have curated a dataset from 6 different centers incorporating more than 300 patients. The dataset includes both single frame and sequence data with 3446 annotated polyp labels with precise delineation of polyp boundaries verified by six senior gastroenterologists. Such pixel-level annotation of lesions is crucial for especially Paris II a-c polyps > 10mm. To our knowledge, this is the most comprehensive detection and pixel-level segmentation dataset curated by a team of computational scientists and expert gastroenterologists. Attentive splits are provided to test the generalization capability of methods for improved clinical applicability but not enforced. The dataset also is suitable for exploring federated learning and training of other time-series models. This dataset has been originated as the part of the Endocv2021 challenge aimed at addressing generalisability in polyp detection and segmentation. In this paper, we provide comprehensive insight into data construction and annotation strategies, annotation quality assurance and technical validation for our extended EndoCV2021 dataset which we refer to as *PolypGen*.

Background and summary

About 1.3 million new cases of colorectal cancer (CRC) are detected yearly in the world, with about 51% mortality rate, and CRC is the third most common cause of cancer mortality¹. Approximately, 90% of CRCs result from slow transformation of the main benign precursors, adenomas or serrated polyps to CRC, but only a minority of them progress to CRC^{2,3}. It is particularly challenging to assess the malignant potential for lesions smaller than 10 mm. As a consequence most detected lesions are removed with subsequent CRC mortality reduction⁴. The removal of the lesions depends also of an exact delineation of the boundaries to assure complete resection. If the lesions are detected and completely removed at a precancerous stage, the mortality is nearly 0%⁵. Unfortunately, there is a considerable limitation related to various human skills^{6,7} confirmed in a recent systematic review and meta-analysis demonstrating miss rates of 26% for adenomas, 9% for advanced adenomas and 27% for serrated polyps⁸. A thorough and detailed assessment of the neoplasia is essential to assess the malignant potential and the appropriate treatment. This assessment is based on size, morphology and surface structure. Currently, the Paris classification, prone to substantial inter-observer variation even among experts, is used to assess the morphology⁹. The surface structure classified by the Kudo pit pattern classification system or the Narrow-Band Imaging International Colorectal Endoscopic (NICE) classification system also help to predict the risk and degree of malignant transformation¹⁰. This classification system may to some extent also predict the histopathological classification into either adenomas, sessile serrated lesions (SSLs), hyperplastic polyps or traditional serrated adenoma (TSA)¹⁰. Unfortunately, these macroscopic classification systems are prone to substantial inter-observer variations, thus a high performing automatic computer-assisted system would be of great importance both to increase detection rates and also reduce inter-observer variability. To develop such a system large segmented image databases are required. While current deep learning approaches have been instrumental in the development of computer-aided diagnosis (CAD) systems for polyp identification and segmentation, most of these trained networks suffer from huge performance gap when out-of-sample data have large domain shifts. On one hand, training models on large multi-center datasets all together can lead to improved generalisation, but at an increased risk of false detection alarms¹¹. On the other hand, training and validation on center-based splits can improve model generalisation. Most reported works are not focused on multi-center data at all. This is mostly because of the lack of comprehensive multi-center and multi-population datasets. In this paper, we present the *PolypGen* dataset that incorporates colonoscopy data from 6 different centers for multiple patient and varied populations. *PolypGen* can be pivotal in algorithm development and in providing more clinically applicable CAD detection and segmentation systems.

Although there are some publicly available datasets for colonoscopic single frames and videos (Table 1), lack of pixel-level annotations and preconditions applied for access of them pose challenges in its wide usability for method development. Many of these datasets are by request which requires approval from the data provider that usually takes prolonged time for approval and the approval is not guaranteed. Similarly, some datasets do not include pixel-level ground truth for the abnormality location which will cause difficulty in development or validation of CAD systems (e.g., El salvador atlas¹² and Atlas of GI Endoscope¹³). Moreover, most of the publicly available datasets include limited number of images frames from one or a few centers only (e.g., datasets provided in ^{14, 15, 15, 16}). To this end, the presented *PolypGen* dataset is composed of a total of 6282 frames including both single and sequence frames. The provided comprehensive dataset consists of 3762 positive sample frames and 2520 negative sample frames collected from six different hospitals comprising of varied population data, endoscopic system and surveillance expert, and treatment procedures for polyp resections. A t-SNE plot for positive samples provided in the **Supplementary Figure 1** demonstrates the diversity of the compiled dataset.

Methods

Study design

Our multi-center polyp detection and segmentation dataset consists of colonoscopy video frames that represent varied patient population imaged at six different centers including Egypt, France, Italy, Norway and the United Kingdom (UK). More than 300 unique patient videos/frames were used for this study. The general purpose of this diverse dataset is to allow robust design of deep learning models and their validation to assess their generalizability capability. In this context, we have proposed different dataset configurations for training and out-of-sample validation and proposed unique generalization assessment metrics to reveal the strength of deep learning methods. Below we provide a comprehensive description of dataset collection, annotation strategies and its quality, ethical guidelines and metric evaluation strategies.

Video acquisition, collection and dataset construction

A consortium of six different medical data centers (hospitals) were built where each data center provided videos and image frames from at least 50 unique patients. The videos and image samples were collected and sent by the senior gastroenterologists involved in this project. The collected dataset consisted of both polyp and normal mucosa colonoscopy acquisitions. To incorporate the nature of polyp occurrences and maintain heterogeneity in the data distribution, the following protocol was adhered for establishing the dataset:

Dataset	Findings	Size	Availability
Kvasir-SEG ¹⁷	Polyps	1000 images [†]	open academic
HyperKvasir ¹⁸	GI findings including polyps	110,079 images and 374 videos	open academic
Kvasir-Capsule ¹⁹	GI findings including polyps [◊]	4,741,504 images	open academic
CVC-ColonDB ²⁰	Polyps	380 images ^{† †}	by request [•]
ETIS-Larib Polyp DB ²¹	Polyps	196 images [†]	open academic
EDD2020 ^{16,22}	GI lesions including polyps	386 images	open academic
CVC-ClinicDB ²³	Polyps	612 images [†]	open academic
CVC-VideoClinicDB ²⁴	Polyps	11,954 images [†]	by request [•]
ASU-Mayo polyp database ²⁵	Polyps	18,781 images [†]	by request [•]
KID ²⁶	Angiectasia, bleeding, inflammations [◊]	2371 images, 47 videos	open academic [•]
Atlas of GI Endoscope ¹³	GI lesions	1295 images	unknown [•]
El salvador atlas ¹²	GI lesions	5071 video clips	open academic [♦]

[†]Including ground truth segmentation masks [‡]Contour [◊]Video capsule endoscopy [•]Not available anymore

[♦]Medical atlas for education with several low-quality samples of various GI findings,

Table 1. An overview of existing gastrointestinal lesion datasets including polyps

1. Single frame sampling from each patient video incorporated different view points
2. Sequence frame sampling consisted of both visible and invisible polyp frames (at most cases) with a minimal gap
3. While single frame data consisted of all polyp instances in that patient, sequence frame data consisted of only a localised targeted polyp
4. Positive sequence included both positive and negative polyp instances but from video with confirmed polyp location while for negative sequence only patient videos with normal mucosa were used

An overview of the number of samples comprising positive samples and negative samples is presented in Figure 1 a. The total positive samples of 3762 frames are released that comprises of 484, 1166, 457, 677, 520 and 484 frames from centers C1, C2, C3, C4, C5 and C6, respectively. These frames consist of 1449 single frames and 1793 sequence frames with majority of sequence data sampled from centers C2 (865), C4 (450), and C6 (250). The number of polyp counts for pixel-level annotation of small ($\leq 100 \times 100$), medium (between $> 100 \times 100$ pixels and $\leq 200 \times 200$ pixels), large ($\geq 200 \times 200$ pixels) sized polyps from each center including no polyp frames but frames in close proximity of polyp are represented as histogram plot (Figure 1 b).

We have provided both still image frames and continuous short video sequence data with their corresponding annotations. The positive and negative samples in the dataset of the polyp generalisation (PolypGen) are further detailed below.

Positive samples

Positive samples consist of video frames from the patient with a diagnosed polyp case. The selected frames may or may not have the polyp in it but may be located near to the chosen frame. Nevertheless, a majority of these frames consists of at least one polyp in the frame. For the sequence positive samples, the continuity of the appearance and disappearance of the polyp similar to real scenario has been taken into account and thus these frames can have a mixture of polyp instances and frames with normal mucosa. Exemplary pixel-level annotations of positive polyp samples for each center and their corresponding bounding boxes are presented in **Supplementary Figure 2**.

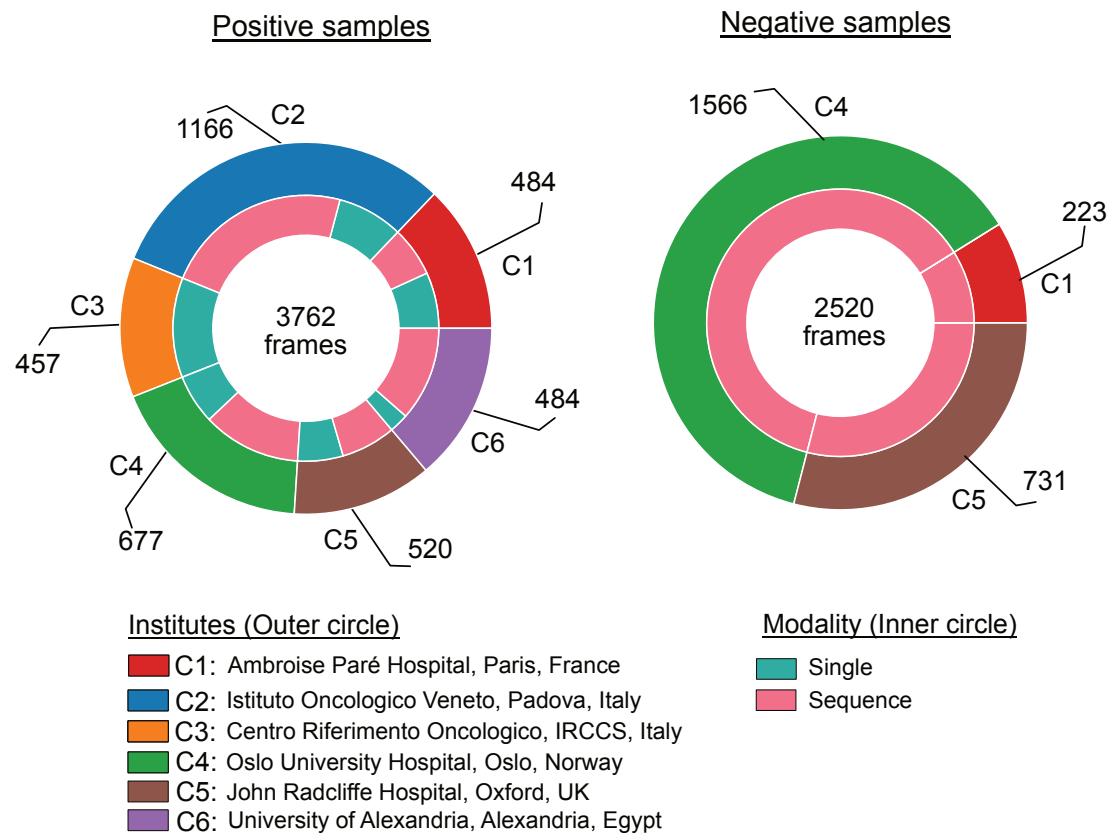
Negative samples

Negative samples mostly refer to the negative sequences released in this dataset. These sequences are taken from patient videos which consisted of confirmed absence of polyps (*i.e.*, normal mucosa) in the acquired videos. It includes cases with anatomies such as colon linings, light reflections and mucosa covered with stool that may be confused with polyps (see Figure 2 and corresponding negative sequence attributes in Table 2).

Annotation strategies and quality assurance

A team of 6 senior gastroenterologists (all over 20 years of experience in endoscopy), two experienced post-doctoral researchers, and one PhD student were involved in the data collection, data sorting, annotation and the review process of the quality of

a. Sample distribution in PolypGen dataset



b. Annotated size-based polyp counts

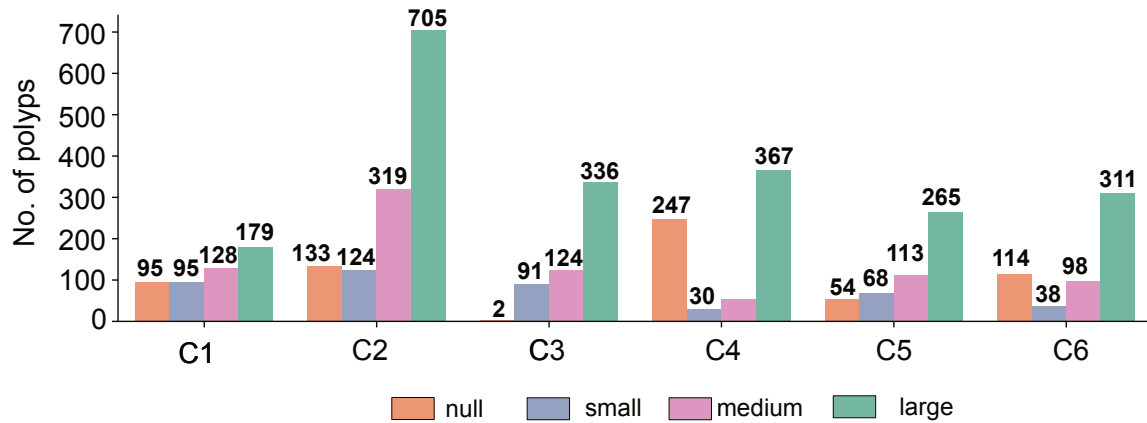


Figure 1. PolypGen dataset: (a) Positive (both single and sequence frames) and negative samples (sequence only) from each center, and (b) polyp size-based histogram plot for positive samples showing variable sized annotated polyps in the dataset (small is $\leq 100 \times 100$ pixels; medium is $> 100 \times 100 \leq 200 \times 200$, and large is $> 200 \times 200$ pixels). Null represents no polyp present in the sample.

annotations. For details on data collection and data sorting please refer to Section **Video acquisition, collection and dataset construction**. All annotations were performed by a team of three experienced researchers using an online annotation tool

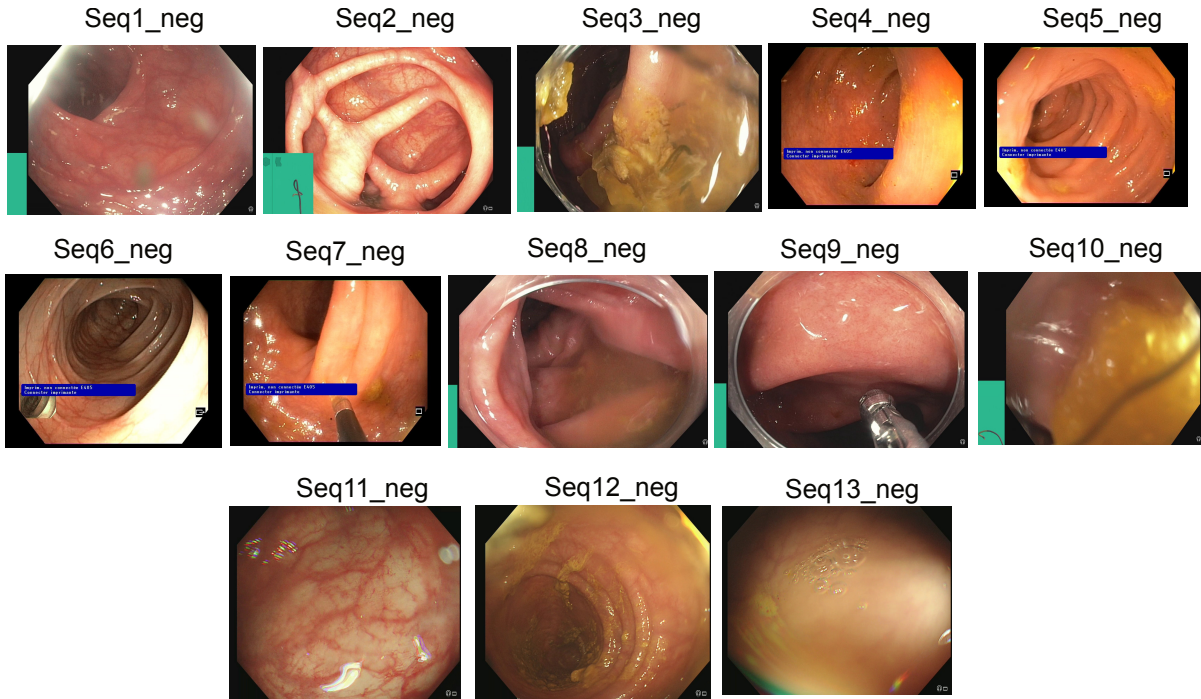


Figure 2. Negative sequence data: Representative samples chosen from each sequence of the provided negative samples data. A summary description is provided in Table 2. Parts of images have been cropped for visualization.

Sequence	Description	Artifact
seq1_neg	Normal vascular pattern	Light reflections in the periphery; not clean lens
seq2_neg	Normal vascular pattern	Contracted bowel; light reflections
seq3_neg	Mucosa not satisfactorily visualized	Stool covers the field of view
seq4_neg	Reduced vascular pattern	Light reflections and small amount of stool
seq5_neg	Reduced vascular pattern	Light reflections
seq6_neg	Normal vascular pattern	Light reflections; biopsy forceps
seq7_neg	Normal vascular pattern	Very close to the luminal wall
seq8_neg	Normal vascular pattern	Blurry; semi-opaque liquid; cap
seq9_neg	Normal vascular pattern	Blurry; semi-opaque liquid; cap
seq10_neg	Not possible to assess the mucosa	Blurry; occluded
seq11_neg	Normal vascular pattern	Light reflections in the periphery; bubble on the lens
seq12_neg	Normal vascular pattern	Not clean lens, mucosa covered by stool
seq13_neg	Probably normal vascular pattern; Not possible to assess the mucosa	Air bubbles; remnant stool; too close to the mucosa, blur, reflections

Table 2. Negative sample sequence summarised attribute: Total of 13 sequences are provided as negative sample sequence for patients with no polyp during colonoscopy examination. These sequences depict different artifacts and varying visibility of vascular pattern and occlusion of mucosa.

called Labelbox¹. Each annotation was later cross validated for accurate segmentation margins by the team and by the center expert. Further, an independent binary review process was then assigned to a senior gastroenterologists, in most cases experts from different centers were assigned. A protocol for manual annotation of polyp was designed to minimise the heterogeneity in the manual delineation process. The set protocols are listed below (refer **Supplementary Figure 2** for final ground truth annotations):

- Clear raised polyps: Boundary pixels should include only protruded regions. Precaution has to be taken when delineating along the normal colon folds

¹<https://labelbox.com>

Centers	System info.	Ethical approval	Patient consenting type
Ambroise Paré Hospital, Paris, France	Olympus Exera 195	N° IDRCB: 2019-A01602-55	Endospectral study
Istituto Oncologico Veneto, Padova, Italy	Olympus endoscope H190	NA	Generic patients consent
Centro Riferimento Oncologico, IRCCS, Italy	Olympus VG-165, CV180, H185	NA	Generic patients consent
Oslo University Hospital, Oslo, Norway	Olympus Evis Exera III, CF 190	Exempted [†]	Written informed consent
John Radcliffe Hospital, Oxford, UK	GIF-H260Z, EVIS Lucera CV260, Olympus Medical Systems	REC Ref: 16/YH/0247	Universal consent
University of Alexandria, Alexandria, Egypt	Olympus Exera 160AL, 180AL	NA	Written informed consent

[†] Approved by the data inspectorate. No further ethical approval was required as it did not interfere with patient treatment

Table 3. Data collection information for each center: Data acquisition system and patient consenting information.

- Inked polyp regions: Only part of the non-inked appearing object delineation
- Polyps with instrument parts: Annotation should not include instrument and is required to be carefully delineated and may form more than one object
- Pedunculated polyps: Annotation should include all raised regions unless appearing on the fold
- Flat polyps: Zooming the regions identified with flat polyps before manual delineation. Also, consulting center expert if needed.

Each of these annotated masks were reviewed by expert gastroenterologists. During this review process, a binary score was provided by the experts depending on whether the annotations were clinically acceptable or not. Some of the experts also provided feedback on the annotation and these images were placed into ambiguous category for further rectification based on expert feedback. These ambiguous category was then jointly annotated by two researchers and further sent for review to one expert. The outcome of these quality checks are provided in Figure 3. It can be observed that large fraction (30.5%) of annotations were rejected (excluding ambiguous batch, total annotations were 2213, among which only 1537 were accepted and 676 frames were rejected). Similarly, the ambiguous batch that included correction of annotations after the first review also recorded 34.17% rejected frames on the second review.

Ethical and privacy aspects of the data

PolypGen data was collected from 6 different centers. Each center was responsible for handling the ethical, legal and privacy of the relevant data. The data collection from each center included either two or all essential steps described below:

1. Patient consenting procedure at each individual institution (required)
2. Review of the data collection plan by a local medical ethics committee or an institutional review board
3. Anonymization of the video or image frames (including demographic information) prior to sending to the organizers (required)

Table 3 illustrates the ethical and legal processes fulfilled by each center along with the endoscopy equipment and recorders used for the data collected.

Data Records

A sub-set of this dataset (from C1 - C5 except C6) forms the dataset of our EndoCV2021 challenge (*Addressing generalisability in polyp detection and segmentation*) training data (<https://endocv2021.grand-challenge.org>), *i.e.*, an event held in conjunction with the IEEE International Symposium on Biomedical Imaging (ISBI 2021), Nice, France. The current released data consists of additional positive and negative frames for both single and sequence data and a 6th center data (C6). The presented version does not consist of training and test splits and users are free to apply their own strategies as applicable to the nature of their work.

The folder structure of the compiled multi-center polyp detection and segmentation dataset is as presented in Figure 4. The main folder “PolypGen” is divided into folders a) Positive and b) Negative. The positive folder is then subdivided (sub-folder level 0) into “Single_Frames_Center_Split” and “Sequence_Frames”. Each of these folders are then further subdivided (sub-folder-1). Single frame data is further categorized as center-wise split “data-C1” to “data-C6”, where C1 representing center 1 and C6 representing the 6th center, while sequence frames are categorized into “seq_1” to “seq_23” (legend color in Figure 4 represents

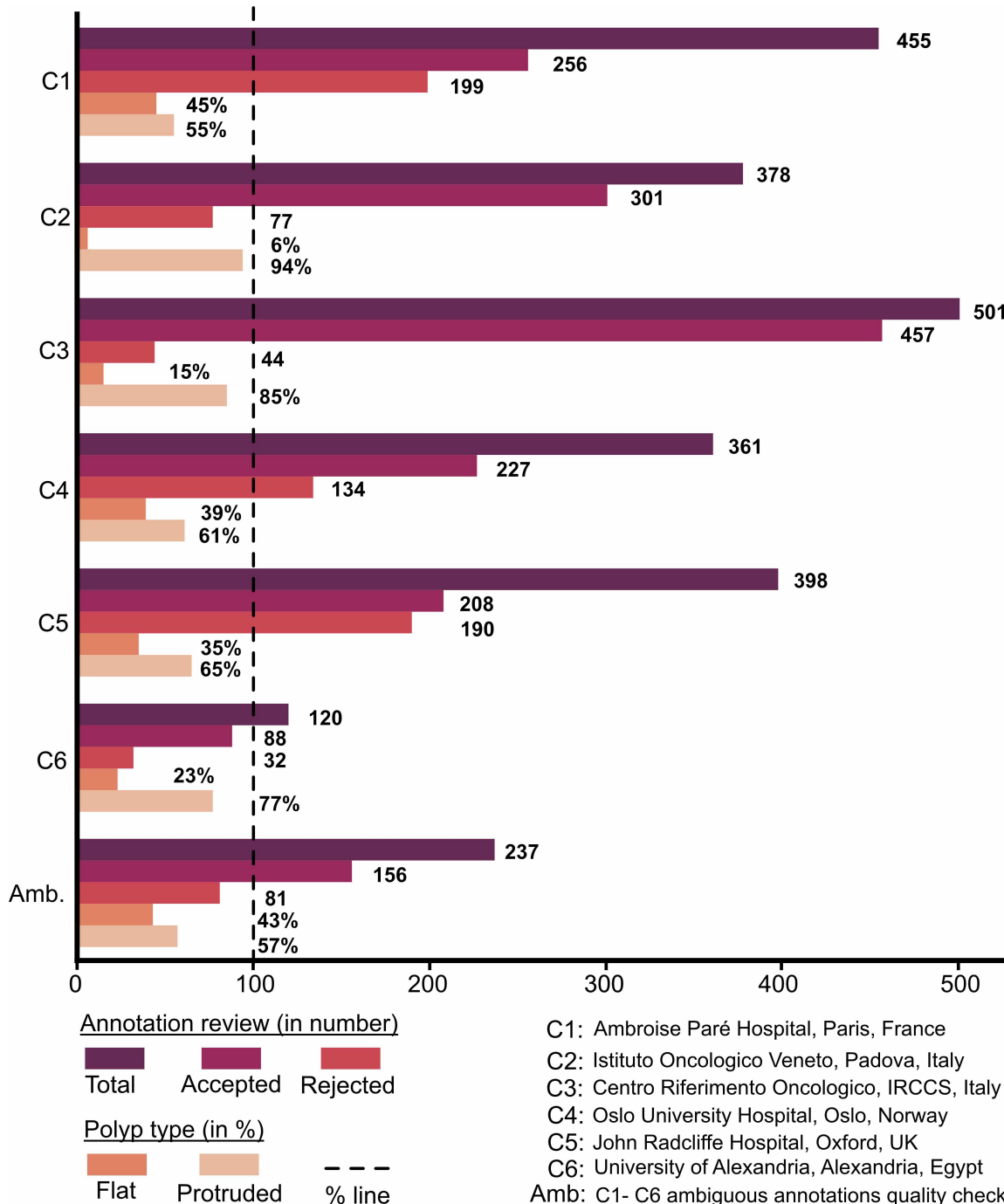


Figure 3. Annotation quality review: Total curated frames along with accepted and rejected frame numbers during annotation quality review by experts for single frame data. Annotated frames with % of flat and protruded polyps categorised during annotation are also provided.

their corresponding center). Finally, a second sub-folder level 2 includes 4 folders consisting of original images (.jpg format), annotated masks (.jpg format), bounding boxes (.txt) in the standard PASCAL VOC format²⁷, and images with box overlay (.jpg). No mix of centerwise sequence is done in any of the sequence data, and the data can consist of both positive negative polyp image samples. No polyp in positive samples mask empty bounding box files and mask with null values. Both masks and bounding box overlaid images are of same size as that of the original images. The negative frames folder on the other hand does consist of only sequence frames, i.e., sub-folder level 0 only as these sequence samples consists of patients with no polyps during the surveillance. To further assist the users, we have also provided the folder structure inside the main folder

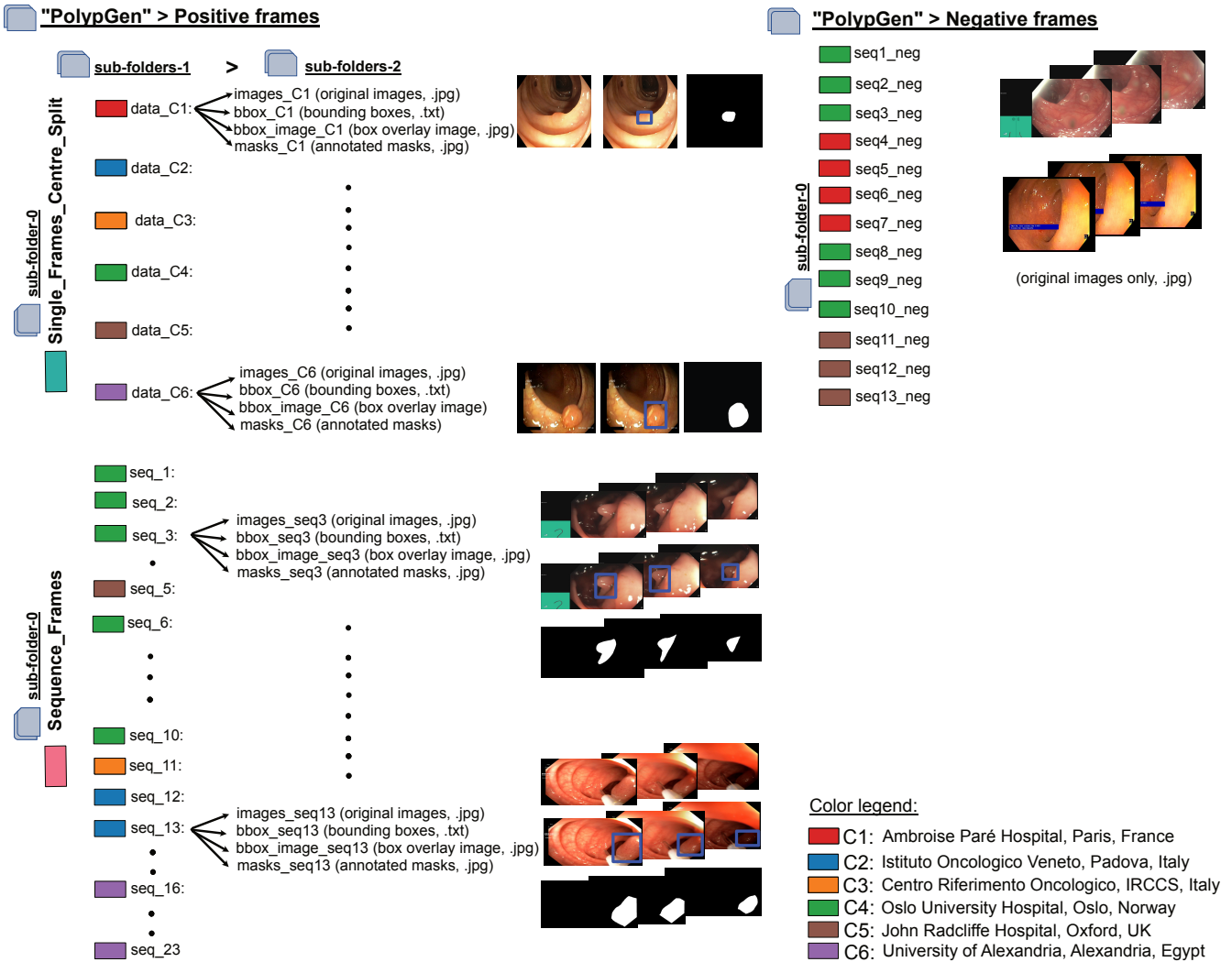


Figure 4. Folder structure: PolypGen dataset is divided into two folders – positive frames and negative frames. Later, it is divided into three different levels for positive frames and only one level for negative samples. (On left) Sub-folder structure with different folder names and the format of data present in each sub-folder 2 is provided. Sample images are also shown. (On right) Sub-folders present in negative folder is shown with two sample sequences (from center 4 and center 1). Each data source center is shown as color legends.

“PolypGen”. The size of images provided in the dataset can range from 384×288 pixels to 1920×1080 pixels. The size of masks correspond to the size of the original images, however, the polyp sizes in the provided dataset is variable (as indicated in Figure 1).

Technical Validation

For the technical validation, we have included single frames data (1449 frames) from five centers (C1 to C5) in our training set and tested on out-of-sample C6 data on both single (88 frames) and sequence frames (432 frames). Such out-of-sample testing on a completely different population and endoscopy device data allows to comprehensively provide evidence of generalisability of current deep learning methods. The training set was split into 80% training only and 20% validation data. Here, we take most commonly used methods for segmentation in the biomedical imaging community^{28–32}, including that for polyps. For reproducibility, we have included the train-validation split as *.txt* files as well in the *PolypGen* dataset folder. However, users can choose any set of different combined training or split training schemes for generalisation tests as they prefer, e.g., training on random three centers and testing on remaining three centers. Also, the dataset is suitable for federated learning (FL) approaches³³ that uses decentralised training and allow to aggregate the weights from the central server for improved and

Method	JI \uparrow	DSC \uparrow	F2 \uparrow	PPV \uparrow	Recall \uparrow	Acc. \uparrow	$d_{AHD} \downarrow$	FPS \uparrow
FCN8 ²⁸	0.68 \pm 0.30	0.76 \pm 0.30	0.75 \pm 0.31	0.90 \pm 0.15	0.74 \pm 0.31	0.97	10.69	44
U-Net ²⁹	0.55 \pm 0.34	0.63 \pm 0.36	0.64 \pm 0.36	0.76 \pm 0.31	0.66 \pm 0.37	0.96	13.89	21
PSPNet ³⁰	0.72 \pm 0.27	0.80 \pm 0.26	0.79 \pm 0.27	0.88 \pm 0.20	0.79 \pm 0.28	0.98	10.39	31
DeepLabV3+ ³¹ (ResNet50)	0.75 \pm 0.28	0.81 \pm 0.27	0.80 \pm 0.28	0.92 \pm 0.17	0.79 \pm 0.29	0.98	9.95	47
ResNetUNet ^{29,32} (ResNet34)	0.73 \pm 0.29	0.79 \pm 0.29	0.77 \pm 0.29	0.92 \pm 0.20	0.78 \pm 0.29	0.98	10.04	87
DeepLabV3+ ³¹ (ResNet101)	0.75 \pm 0.28	0.82 \pm 0.27	0.80 \pm 0.27	0.92 \pm 0.18	0.81 \pm 0.27	0.98	9.67	33
ResNetUNet ^{29,32} (ResNet101)	0.74 \pm 0.29	0.80 \pm 0.28	0.80 \pm 0.28	0.93 \pm 0.14	0.80 \pm 0.29	0.98	10.10	40

JC: Jaccard coefficient DSC: Dice coefficient F2: Fbeta-measure, with $\beta = 2$ PPV: positive predictive value

Acc.: overall accuracy d_{AHD} : Average Hausdorff distance FPS: frames per second

Table 4. Performance evaluation of SOTA segmentation methods on 88 single frames from center 6 in an out-of-sample generalisation task. Top two methods are presented in bold.

generalisable model without compromising data privacy.

Benchmarking of state-of-the-art methods

To provide generalisation capability of some state-of-the-art (SOTA) methods, we have used a set of popular and well-established semantic segmentation CNN models on our PolypGen dataset. Each model was run for nearly 500 epochs with batch size of 16 for image size of 512×512 . All models were optimised using Adam with weight decay of 0.00001 learning rate of 0.01 and allowing the best model to be saved after 100 epochs. Classical augmentation strategies were used that included scaling (0.5, 2.0), random cropping, random horizontal flip and image normalisation. All models were run on Quadro RTX6000.

Evaluation metrics for segmentation.

We compute standard metrics used for assessing segmentation performances that includes Jaccard Index ($JI = \frac{TP}{TP+FP+FN}$), F1-score (aka Dice similarity coefficient, DSC), F2-score, precision (aka positive predictive value, PPV or $p = \frac{TP}{TP+FP}$), recall ($r = \frac{TP}{TP+FN}$), and overall accuracy ($Acc. = \frac{TP+TN}{TP+TN+FP+FN}$) that are based on true positives (TP), false positives (FP), true negatives (TN), and false negatives (FN) pixel counts. Precision-recall tradeoff is also given by the Dice similarity coefficient (DSC) or F1-score and F2-scores:

$$F_\beta = (1 + \beta^2) \cdot \frac{p \cdot r}{(\beta^2 \cdot p) + r}, \quad (1)$$

where F_β -score is computed as weighted harmonic means of precision and recall.

Another commonly used segmentation metric that is based on the distance between two point sets, here ground truth (G) and estimated or predicted (E) pixels, to estimate ranking errors is the average Hausdorff distance (d_{AHD}) and defined as:

$$d_{AHD}(G, E) = \left(\frac{1}{G} \sum_{g \in G} \min_{e \in E} d(g, e) + \frac{1}{E} \sum_{e \in E} \min_{g \in G} d(g, e) \right) / 2. \quad (2)$$

Polyp segmentation

The U-Net architecture developed by Ronnerberger et al.²⁹ has shown tremendous success in medical image segmentation³⁴ including endoscopy^{16,35}. PSPNet³⁰ is designed to incorporate global context information for the task of scene parsing. Similarly, dilated convolutions enabled the construction of semantic segmentation networks to effectively control the size of the receptive field that was incorporated in an a family of very effective semantic segmentation architectures, collectively named DeepLab³¹. All of these networks has been explored for polyp segmentation in literature³⁶⁻³⁸. Here, we benchmark our dataset on these popular deep learning model architectures. Out-of-sample generalisation results for both single frame (Table 4) and sequence data (Table 5) has been included in our technical validation of the presented data.

Validation Summary

Our technical validation suggest that DeepLabV3+ with ResNet101 has the best performance on most metrics except for FPS suggesting larger latency in inference (Table 4 and Table 5). The highest score was 0.82 for DSC and the least 9.67 for d_{AHD}

Method	JC \uparrow	DSC \uparrow	F2 \uparrow	PPV \uparrow	Recall \uparrow	Acc. \uparrow	$d_{AHD} \downarrow$
FCN8 ²⁸	0.56 \pm 0.37	0.62 \pm 0.38	0.59 \pm 0.37	0.88 \pm 0.28	0.63 \pm 0.36	0.95	9.84
UNet ²⁹	0.43 \pm 0.37	0.50 \pm 0.39	0.47 \pm 0.39	0.68 \pm 0.41	0.62 \pm 0.37	0.95	11.22
PSPNet ³⁰	0.58 \pm 0.38	0.64 \pm 0.38	0.61 \pm 0.38	0.84 \pm 0.33	0.68 \pm 0.35	0.96	9.84
DeepLabV3+ ³¹ (ResNet50)	0.60 \pm 0.37	0.67 \pm 0.37	0.64 \pm 0.37	0.85 \pm 0.31	0.71 \pm 0.33	0.96	9.63
ResNetUNet ^{29,32} (ResNet34)	0.59 \pm 0.37	0.66 \pm 0.38	0.63 \pm 0.3808	0.8674 \pm 0.2998	0.70 \pm 0.35	0.96	9.78
DeepLabV3+ ³¹ ResNet101	0.65 \pm 0.37	0.71 \pm 0.37	0.68 \pm 0.37	0.90 \pm 0.26	0.73 \pm 0.34	0.97	9.08
ResNetUNet ^{29,32} (ResNet101)	0.65 \pm 0.37	0.70 \pm 0.37	0.68 \pm 0.37	0.92 \pm 0.22	0.71 \pm 0.35	0.96	9.20

JC: Jaccard coefficient DSC: Dice coefficient F2: Fbeta-measure, with $\beta = 2$ PPV: positive predictive value

Acc.: overall accuracy d_{AHD} : Average Hausdorff distance

Table 5. Performance evaluation of SOTA segmentation methods on 432 sequence frames from center 6 in an out-of-sample generalisation task. Top two methods are presented in bold.

with DeepLabV3+ with ResNet101 on single frame data. However, the second best inference speed (FPS of 47) and score (DSC = 0.81, $d_{AHD} = 9.95$) was obtained again using DeepLabV3+ but with ResNet50 backbone. Similarly, for sequence C6 out-of-sample test generalisation the highest score of 0.65 for DSC with highest recall of 0.73 and the least 9.08 for d_{AHD} was obtained with DeepLabV3+ with ResNet101 backbone. With the same ResNet101 backbone ResUNet resulted in very close performance of 0.65 DSC but with highest precision on 0.92 and d_{AHD} of 9.20. However, even with the same ResNet101 backbone ResUNet (40 FPS) has better speed compared to DeepLabV3+ (33 FPS).

Limitations of the dataset

The positive sample catalogue consists of both polyp and non-polyp images for completeness (see Figure 1 b). The entire dataset has been carefully reviewed by senior gastroenterologists, however, there may be some unseen discrepancies. The accuracy, reliability and completeness of the annotations may be subjective to the annotators.

Usage Notes

All released dataset has been published under Creative Commons Attribution-NonCommercial-ShareAlike 4.0 (CC-BY-NC-SA 4.0). Dataset can only be used for educational and research purposes and must cite this paper.

The released dataset has been divided into positive and negative samples. Additionally, positive samples are divided into single frames and sequence frames. Users are free to use the samples according to their method demand. For example, for fully convolutional neural networks we adhere to the use of positive samples as done in our technical validation, while for the recurrent techniques that exploit temporal information users may use both positive and negative sequence data.

Code availability

To help users with the evaluate the generalizability of detection and segmentation method a code is available at: https://github.com/sharibox/EndoCV2021-polyp_det_seg_gen. The code also consists of inference codes that to assist in center-based split analysis.

Data availability

The dataset is currently under embargo period and will be immediately released under Creative Commons Attribution-NonCommercial-ShareAlike 4.0 (CC-BY-NC-SA 4.0) after the publication of EndoCV2021 joint journal paper. This paper version will be updated with the data link and additional details.

References

- Bray, F. *et al.* Global cancer statistics 2018: GLOBOCAN estimates of incidence and mortality worldwide for 36 cancers in 185 countries. *CA Cancer J Clin.* **68**, 394–424 (2018).
- Leslie, A., Carey, F., Pratt, N. & Steele, R. The colorectal adenoma–carcinoma sequence. *Br. J. Surg.* **89**, 845–860 (2002).

3. Loeve, F. *et al.* National polyp study data: evidence for regression of adenomas. *Int. journal cancer* **111**, 633–639 (2004).
4. Kaminski, M. F. *et al.* Increased rate of adenoma detection associates with reduced risk of colorectal cancer and death. *Gastroenterology* **153**, 98–105 (2017).
5. Brenner, H., Kloor, M. & Pox, C. P. Colorectal cancer. *Lancet* **383**, 1490–502, [10.1016/S0140-6736\(13\)61649-9](https://doi.org/10.1016/S0140-6736(13)61649-9) (2014).
6. Hetzel, J. T. *et al.* Variation in the detection of serrated polyps in an average risk colorectal cancer screening cohort. *The Am. journal gastroenterology* **105**, 2656 (2010).
7. Kahi, C. J., Hewett, D. G., Norton, D. L., Eckert, G. J. & Rex, D. K. Prevalence and variable detection of proximal colon serrated polyps during screening colonoscopy. *Clin. Gastroenterol. Hepatol.* **9**, 42–46 (2011).
8. Zhao, S. *et al.* Magnitude, risk factors, and factors associated with adenoma miss rate of tandem colonoscopy: A systematic review and meta-analysis. *Gastroenterology* **156**, 1661–1674 e11, [10.1053/j.gastro.2019.01.260](https://doi.org/10.1053/j.gastro.2019.01.260) (2019).
9. Van Doorn, S. C. *et al.* Polyp morphology: an interobserver evaluation for the paris classification among international experts. *Am. J. Gastroenterol.* **110**, 180–187 (2015).
10. Saito, Y., Wada, Y., Ikematsu, H. *et al.* Multicenter trial to unify magnified nbi classification using web test system. *Intestine* **17**, 223–31 (2013).
11. Liu, W., Zhang, Y., Bian, X. & et al. Study on detection rate of polyps and adenomas in artificial-intelligence-aided colonoscopy. *Saudi J Gastroenterol.* **26**, 13–19 (2020).
12. <https://www.gastrointestinalatlas.com/english/english.html>.
13. Stiegmann, G. V. Atlas of Gastrointestinal Endoscopy. *Arch. Surg.* **123**, 1026–1026, [10.1001/archsurg.1988.01400320112031](https://doi.org/10.1001/archsurg.1988.01400320112031) (1988).
14. <http://www.endoatlas.org/index.php?page=home>.
15. Mesejo, P. *et al.* Computer-aided classification of gastrointestinal lesions in regular colonoscopy. *IEEE transactions on medical imaging* **35**, 2051–2063 (2016).
16. Ali, S. *et al.* Deep learning for detection and segmentation of artefact and disease instances in gastrointestinal endoscopy. *Med. Image Analysis* **70**, 102002, [10.1016/j.media.2021.102002](https://doi.org/10.1016/j.media.2021.102002) (2021).
17. Jha, D. *et al.* KVASIR-SEG: A segmented polyp dataset. In *International Conference on Multimedia Modeling*, 451–462 (Springer, 2020).
18. Borgli, H. *et al.* Hyperkvasir, a comprehensive multi-class image and video dataset for gastrointestinal endoscopy. *Sci. Data* **7**, 1–14 (2020).
19. Smedsrud, P. H. *et al.* Kvasir-capsule, a video capsule endoscopy dataset. *Sci. Data* **8**, 1–10 (2021).
20. Bernal, J., Sánchez, J. & Vilarino, F. Towards automatic polyp detection with a polyp appearance model. *Pattern Recognit.* **45**, 3166–3182 (2012).
21. Silva, J., Histace, A., Romain, O., Dray, X. & Granado, B. Toward embedded detection of polyps in wce images for early diagnosis of colorectal cancer. *Int. journal computer assisted radiology surgery* **9**, 283–293 (2014).
22. Ali, S. *et al.* Endoscopy disease detection challenge 2020. *arXiv preprint arXiv:2003.03376* (2020).
23. Bernal, J. *et al.* Wm-dova maps for accurate polyp highlighting in colonoscopy: Validation vs. saliency maps from physicians. *Comput. Med. Imaging Graph.* **43**, 99–111 (2015).
24. Bernal, J. & Aymeric, H. MICCAI endoscopic vision challenge polyp detection and segmentation (2017).
25. Tajbakhsh, N., Gurudu, S. R. & Liang, J. Automated polyp detection in colonoscopy videos using shape and context information. *IEEE transactions on medical imaging* **35**, 630–644 (2015).
26. Koulaouzidis, A. *et al.* Kid project: an internet-based digital video atlas of capsule endoscopy for research purposes. *Endosc. international open* **5**, E477 (2017).
27. Everingham, M., Van Gool, L., Williams, C. K. I., Winn, J. & Zisserman, A. The PASCAL Visual Object Classes Challenge 2012 (VOC2012) Results. <http://www.pascal-network.org/challenges/VOC/voc2012/workshop/index.html>.
28. Long, J., Shelhamer, E. & Darrell, T. Fully convolutional networks for semantic segmentation. In *Proceedings of the IEEE conference on computer vision and pattern recognition*, 3431–3440 (2015).
29. Ronneberger, O., Fischer, P. & Brox, T. U-net: Convolutional networks for biomedical image segmentation. In *International Conference on Medical image computing and computer-assisted intervention*, 234–241 (Springer, 2015).

30. Zhao, H., Shi, J., Qi, X., Wang, X. & Jia, J. Pyramid scene parsing network. In *Proceedings of the IEEE conference on computer vision and pattern recognition*, 2881–2890 (2017).
31. Chen, L.-C., Zhu, Y., Papandreou, G., Schroff, F. & Adam, H. Encoder-decoder with atrous separable convolution for semantic image segmentation. In *Proceedings of the European conference on computer vision (ECCV)*, 801–818 (2018).
32. He, K., Zhang, X., Ren, S. & Sun, J. Deep residual learning for image recognition. In *Proceedings of the IEEE conference on computer vision and pattern recognition*, 770–778 (2016).
33. Konecný, J., McMahan, H. B., Ramage, D. & Richtárik, P. Federated optimization: Distributed machine learning for on-device intelligence. *ArXiv* **abs/1610.02527** (2016).
34. Sevastopolsky, A. Optic disc and cup segmentation methods for glaucoma detection with modification of U-Net convolutional neural network. *Pattern Recognit. Image Analysis* **27**, 618–624 (2017).
35. Ali, S. *et al.* An objective comparison of detection and segmentation algorithms for artefacts in clinical endoscopy. *Sci. Reports* **10**, 2748, [10.1038/s41598-020-59413-5](https://doi.org/10.1038/s41598-020-59413-5) (2020).
36. Guo, Y., Bernal, J. & J Matuszewski, B. Polyp segmentation with fully convolutional deep neural networks—extended evaluation study. *J. Imaging* **6**, 69 (2020).
37. Jha, D. *et al.* Real-time polyp detection, localization and segmentation in colonoscopy using deep learning. *IEEE Access* **9**, 40496–40510 (2021).
38. Nguyen, N.-Q., Vo, D. M. & Lee, S.-W. Contour-aware polyp segmentation in colonoscopy images using detailed upsampling encoder-decoder networks. *IEEE Access* (2020).

Acknowledgements

The research was supported by the National Institute for Health Research (NIHR) Oxford Biomedical Research Centre (BRC). The views expressed are those of the authors and not necessarily those of the NHS, the NIHR or the Department of Health. S. Ali and JE. East is supported by NIHR Oxford BRC. D. Jha is funded by PRIVATON project and J. Rittscher by Ludwig Institute for Cancer Research and EPSRC Seebibyte Programme Grant.

Author contributions statement

S. Ali conceptualized, initiated, and coordinated the work. He led the data collection, curation, and annotation processes and conducted most of the analyses and writing of the paper. T. de Lange assisted in writing of the introduction, clinical correctness of the paper and provided feedback regarding description of sequences presented in the manuscript. D. Jha and N. Ghatwary assisted in data annotation and parts of technical validation. S. Realdon, R. Cannizzaro, O. Salem, D. Lamarque, C. Daul, T. de Lange, M. Riegler, P. Halvorsen, K. Anonsen, J. Rittscher, and J. East were involved directly or indirectly in facilitating the video and image data from their respective centers. Senior gastroenterologists and collaborators S. Realdon, R. Cannizzaro, O. Salem, D. Lamarque, T. de Lange, and J. East provided timely review of the annotations and required feedback during dataset preparation. All authors read the manuscript, provided substantial feedback, and agreed for submission.

Competing interests

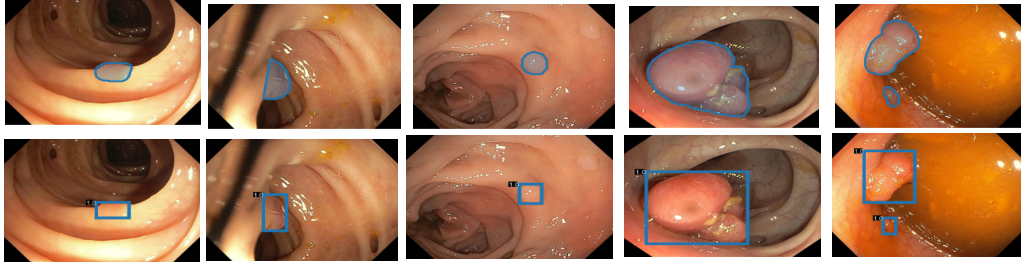
The authors declare that they have no known competing financial interests or personal relationships that could have appeared to influence the work reported in this paper.

Supplementary material

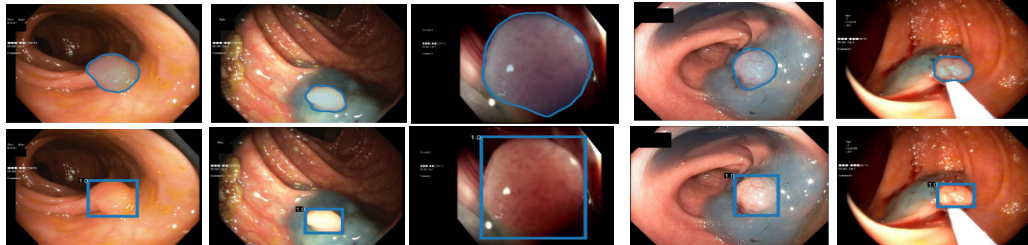


Figure 1. t-SNE plot for positive samples: 2D t-SNE embedding of the “PolypGen” dataset based on deep autoencoder extracted features. Each point is an image in the positive samples of the dataset. For each of the 7 boxed regions (dashed black lines) 25 images were randomly sampled for display in a 5×5 image grid. Here, for the 1st and the 7th boxed regions represent mostly the sequence data. Interestingly, the 3rd and the 6th boxed regions mostly represent both polyp and non-polyp data from different provided sequences but belonging to mostly same patient. Similarly, the remaining box areas illustrate the diverse image samples.

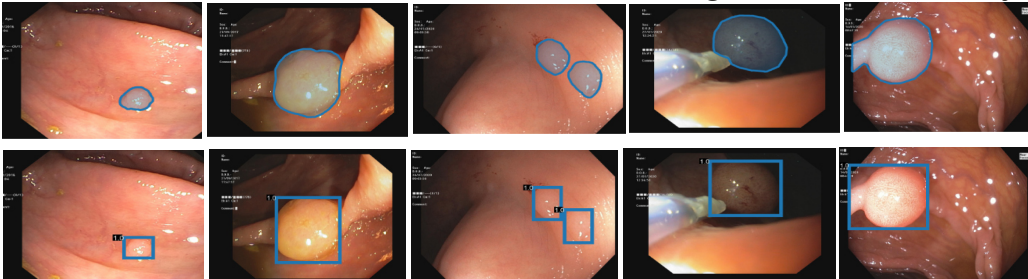
 C1: Ambroise Paré Hospital, Paris, France



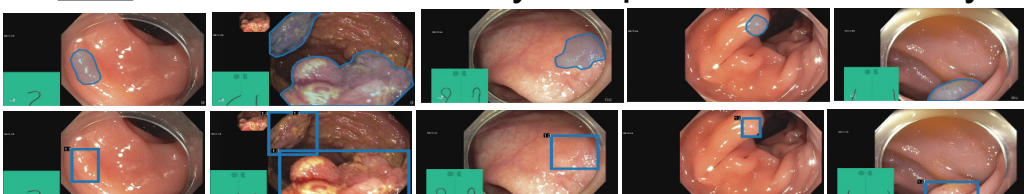
 C2: Istituto Oncologico Veneto, Padova, Italy



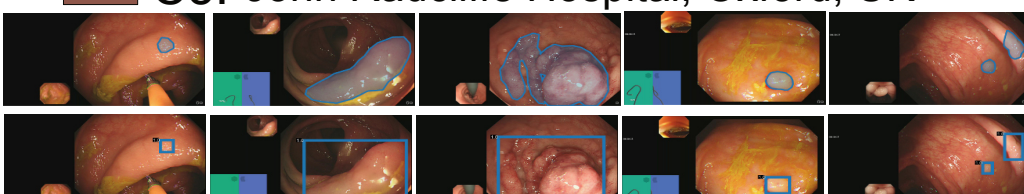
 C3: Centro Riferimento Oncologico, IRCCS, Italy



 C4: Oslo University Hospital, Oslo, Norway



 C5: John Radcliffe Hospital, Oxford, UK



 C6: University of Alexandria, Alexandria, Egypt



Figure 2. Sample polyp annotations from each center: Segmentation area with boundaries and corresponding bounding box/boxes overlaid images from all six centers. Samples include both small sized polyp ($< 10000\text{ pixels}$) including some flat polyp samples to large sized ($\geq 40000\text{ pixels}$) polyps and polyps during resection procedure such as polyps with blue dyes.